COMPARISON OF RADIAL MAGNETIC BEARING DESIGNS

Anthony S. Kondoleon
William P. Kelleher

Draper Laboratory
555 Technology Square
Cambridge, Ma 02139

ABSTRACT

The initial design of an active magnetic bearing actuator is critical for a successful magnetic suspension. The sizing of the stators and rotors is a vital step for maintaining a favorable weight to load capacity ratio for the magnetic suspension. Sizing the stators and rotors for minimum running losses during high-speed operation is a challenge all designers face. This paper presents results from recently completed analyses for running loss determination in radial magnetic bearings, and presents how these results are used in the initial design phase for radial magnetic bearings. Comparisons of flux density versus speed for various heteropolar radial flux distribution designs and a comparison of rotating loss versus load for various radial pole counts are also presented.

INTRODUCTION

Designing a radial magnetic bearing actuator for low loss and high load capacity is a challenge. Tests carried out (ref. 1) have provided insight into the nature of rotating losses in these actuators. Combining these results with design procedures (ref. 2) provides a means for determining the basic parameters of the radial bearing actuator for the initial design tradeoff comparisons. The basic design and analysis of a radial magnetic bearing actuator is presented along with magnetic FEM results. The results from the rotating loss tests and the basic equations used to determine rotor losses are then explained. The two procedures are combined for first order calculation of bearing sizing and rotor loss determination required in any initial design tradeoff study. Results are presented from this procedure as it relates to both rotor loss and bearing capacity determination.

MAGNETIC BEARING ACTUATOR SIZING

The basic equation (ref. 3) used to determine the pole area required to magnetically support an object is:

$$\text{Pole Force (F)} = 8260 * \text{Pole Area (A)} * B^2 \qquad [1]$$

where F is in Newton, A is in mm^2 and B is in Tesla. Assuming B in the air gap and the B in the material are approximately the same, then the following equation (4) holds:

$$N * I = B * g_o / \mu_o \qquad [2]$$

where g_o is the air gap length (meters), $\mu_o = 4\pi * 10^{-7}$ (Henrys / meter), N is the number of turns and I is the current (amps). The inductance of a coil and the relationship of inductance, voltage and current are:

$$L = N^2 * \mu_o * A / g_o \qquad [3]$$

$$V / L = dI / dt \qquad [4]$$

where L is in Henrys, V is in volts and t is in seconds.

These four equations when used together are the first steps in determining the size of a magnetic actuator. These equations also show that while all the equations are independent, when some parameters are chosen, then others become dependent. As an example, if the pole force and the maximum flux density are chosen, then the pole area is calculated using [1]. For a given air gap and flux density, the required NI is calculated using [2]. Given a maximum current, the number of turns is determined using [2] and with the number of turns the inductance of the coil is calculated using [3]. For a given voltage, the maximum slew rate of the actuator is calculated using [4].

RADIAL MAGNETIC ROTOR LOSSES

Rotor losses can be separated into three families, losses due to eddy currents, losses due to rotating hysteresis and losses due to alternating hysteresis effects. These three effects are influenced by the magnetic flux density in the material, the shape of the magnetic field, the type of material, mass of the rotor and the lamination thickness. Kasarda (ref. 1) has proposed the following equations for these three losses.

The equation for power loss in a rotor due to eddy currents is:

$$P_e = \frac{\pi^2 d^2 B_{max}^2 f_{eff}^2 M_{vec} (10^{-6})}{6\rho} \left(\text{watts / cm}^3\right) \qquad [5]$$

d = rotor lamination thickness (meters), ρ = resistively (Ω-m) and M_{vec} is the effective volume coefficient. The effective frequency is determined by the rotational speed of the rotor times the number of pole edges:

$$f_{eff} = \frac{N \times n_e}{60} \qquad [6]$$

where N = rotational speed of the rotor in rpm and n_e = number of stator pole edges, 32 for a 16 pole configuration and 16 for an 8 pole configuration.

The equation for the alternating hysteresis power loss component is:

$$P_{ha} = 10^{-7} \eta f_{eff} \left(10000 \times B_{max}\right)^k M_{vah} \left(\text{watts / cm}^3\right) \qquad [7]$$

The hysteresis coefficient, _ , has a proposed value of approximately 0.00046 and the exponent, k, has an approximate value of 1.6 for flux densities (B) in the range of 0.15 to 1.20 Tesla.

The proposed equation for the rotational hysteresis power loss component is:

$$P_{hr} = 10^{-7} [3000.0 \times B_{max} - 500.0] f_r M_{vrh} \quad (\text{Watts/cm}^3) \qquad [8]$$

Where B_{max} is the maximum flux density in Tesla, f_r is the effective frequency in Hz, and M_{vrh} is the effective volume coefficient for the rotational hysteresis calculation. The effective frequency for the rotational hysteresis is:

$$f_r = \frac{N \times n_l}{60} \qquad [9]$$

where N = rotational speed of the rotor in rpm and n_l = the number of flux loops experienced by the journal during one revolution, 8 for 16 pole configuration, 4 for an 8 pole configuration.

The above equations show a basic fact of magnetic bearing design: the loss in the bearing is a function of both maximum flux density and the mass of the rotor. While flux density on the rotor surface produces force, flux density inside the rotor produces loss. Reducing the flux density level inside the bearing and reducing the mass of the rotor at the same time will produce a design which will be low in loss and weight efficient.

RADIAL BEARING FLUX PATHS

The flux paths for a four-pole heteropolar radial bearing are shown in Figure 1. As shown by Figure 1, the flux leaving or entering the pole is twice that of the back iron and the rotor. If the flux density in all the material is desired to be at the same level, then the poles should be twice the cross sectional areas of the rotor and the back iron.

When the actuator poles become greater than four, the flux paths will differ depending on the polarity of the pole configurations. Two heteropolar actuator configurations used are the alternating pole (NSNS) and the pole pair (NNSS) configurations. The flux paths for these two eight-pole configurations, in the bias condition (NI = 200), are shown in Figures 2 and 3.

RADIAL BEARING FINITE ELEMENT MODELING

Finite element modeling was performed on the hetro-polar configurations shown in Figures 2 and 3. The dimensions of the design modeled are shown in Table I. While the flux density on the rotor surface is the same in the bias condition for the two configurations under the poles, (Figures 4 and 5), the pattern of the flux density is vastly different. Figures 6 and 7 show the flux density at the middle of the rotor for the two configurations. Both configurations have the same maximum flux density in and on the rotor, but with a different profile. Figures 8 and 9 show the flux density in the stator between poles 1 and 8. While the flux density under the poles on the rotor is the same, the flux density in the stator is approximately 200% higher for the pole pair configuration than the alternating pole configuration.

Figures 10 and 11 show FEM results of the flux paths for the two configurations in the maximum force condition (NI = 450), four poles on and four poles off. Figures 12 to 15 show the FEM results for the flux density on and in the rotor for the maximum force condition. As in the bias condition, the flux density levels are the same for the two configurations, but the patterns are again different. Figures 16 and 17 shown the flux density in the stator between poles 1 and 8. The flux density in the pole pair configuration is approximately 25% higher than the alternating pole configuration.

COMPARING FINITE ELEMENT MODELING AND POWER LOSS MEASUREMENTS

Kasarda (ref. 1) has shown that at speeds above 3,000 rpm, the loss in the rotors for the two configurations is approximately the same. Below 3,000 rpm, the pole pair configuration had less loss than the alternating pole configuration. This suggests that at high frequencies, the flux density level is more important than the flux density frequency pattern on or in the rotor.

DISTRIBUTED FLUX BEARING DESIGN

From the above analysis, the pole configuration at the same flux density level produces the same loss in the rotors. Reducing the loss by reducing the mass of the rotor is attempted by the distributed flux configuration magnetic bearing shown in Figure 18. The dimension of the magnetic bearing modeled for this configuration is shown in Table I. Figures 19 to 21 show the results of the FEM the flux density levels for this configuration in the bias condition (NI = 200). Figure 22 shows the flux pattern for the maximum force condition (NI = 450) for this configuration. In this configuration, three upper poles are in the full on state, the two horizontal poles are set half the NI value of the full on poles and the last three poles are off. Figures 23 to 25 show the results of the FEM for the flux density levels of this configuration in the full force condition.

COMPARING FINITE ELEMENT CONFIGURATION MODELS

Comparing the FEM results on the rotor for this configuration and the two previous designs, the pattern and the maximum levels of flux density for the bias condition are the same. For the maximum force condition, the levels are the same but the pattern is slightly different. The distributed flux condition produces a more efficient design than the other two hetro-polar designs.

POWER LOSS CALCULATIONS

Using equations 5 to 9, power loss calculations were carried out for the three configurations. For a speed of 30,000 rpm and a flux density level of 1.5 Tesla and a one-inch long rotor, the alternating pole and the pole pair configuration produced a power loss of 420 watts. The same length rotor for the flux distribution configuration produced a power loss of 250 watts.

The effective volume coefficient (ref. 1) had a uniform bias field at the poles with a small control flux superimposed at the poles for stability. When a heteropolar bearing is fully energized for maximum load capacity, the flux distribution is changed. In the maximum condition, approximately 50% of the bearing contains flux and approximately 50% is flux free. Modification of the preceding effective volume coefficients to account for these conditions was carried out for a series of first order parametric studies. The conditions held constant in the study were the outside diameter of the stator, the inside diameter of the rotor, the magnetic air gap, and the material properties of the rotor and stator.

For a 445 Newton load capacity bearing, Figure 26 shows the effect which setting the flux density to a maximum has on a four-pole design. Since load capacity changes as the square of the flux density, but the rotor mass changes linearly with flux density, the losses go down as the flux goes up. This type of comparison would be useful when a choice of material is required in the design phase of a program, with the only difference being in the flux saturation limit of the materials in question.

Applying the distributed flux configuration to stators with pole counts of 4, 8, 12, and 16, a comparison of rotor loss versus bearing load was made. For a given speed and control flux density (60,000 rpm and 2 Tesla), Figure 27 shows the influence which pole count in the stator has on rotor losses. The higher the pole count, the less rotor mass is required and the rotor losses go down even with increased effective frequency of the magnetic field in the rotor. The limit to the number of poles, which can be designed into a bearing is a function of the skin effect (ref. 7), the volume required for the coils and the overall volume of the bearing.

SUMMARY

This paper presents a first order attempt to size radial bearings for typical applications. A comparison of test data results to proposed rotor loss equations were presented. The use of these equations to understand the different stator pole configurations was shown. As more data become available on the true nature of rotating losses in magnetic bearings, the equations used in this procedure will be updated.

REFERENCES

1. Kasarda, M. E., " The Measurement and Characterization of Power Losses in High Speed Magnetic Bearings", Ph.D. Thesis, University of Virginia, January 1997
2. Kondoleon, A. S., Kelleher, W. P., " Magnetic Bearings at Draper Laboratory", NASA Publication, CP-3336, July 1996
3. Pearman, P. A., *Electrical Machinery and Transformer Technology*, Saunders College Publishing
4. Fitzgerald, A. E., *Electric Machinery*, McGraw-Hill, 5th edition
5. Kondoleon, A. S., Kelleher, W. P., " A Magnetic Bearing Suspension System for High Temperature Gas Turbine Applications", ASME Publication, 97-GT-114, June 1997
6. Hoole, S. H., *Computer Aided Analysis and Design of Electromagnetic Devices*, 1989 Elsevier Publishing
7. Bozorth, R. M., *Ferro-Magnetism*, Van Nostrand Company, 1964, 8th edition

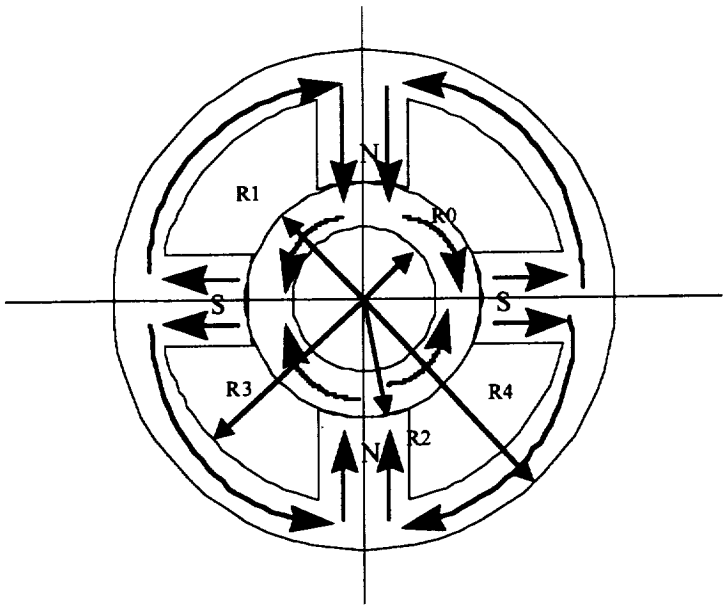

Figure 1 Flux Path for a Four Pole Radial Bearing

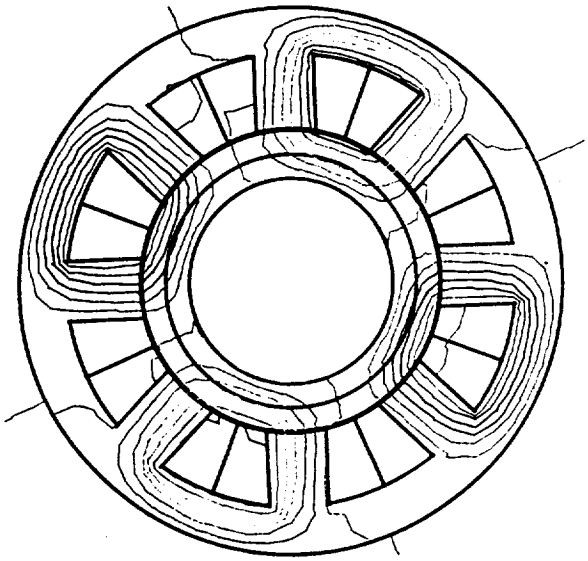

Figure 2 Flux Path for 8 Pole Pair Bias Configuration

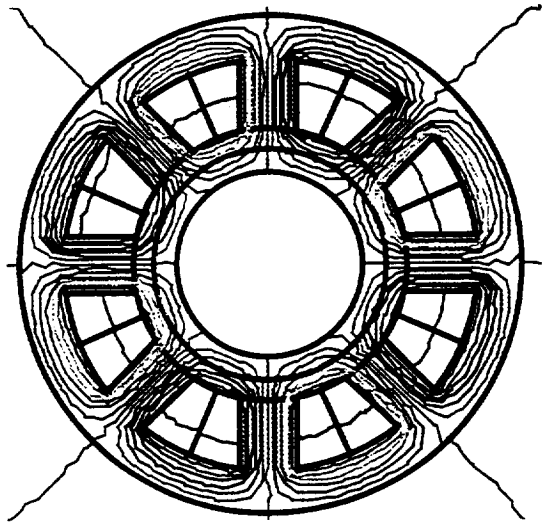

Figure 3 Flux Path for Alternating 8 Pole Bias Configuration

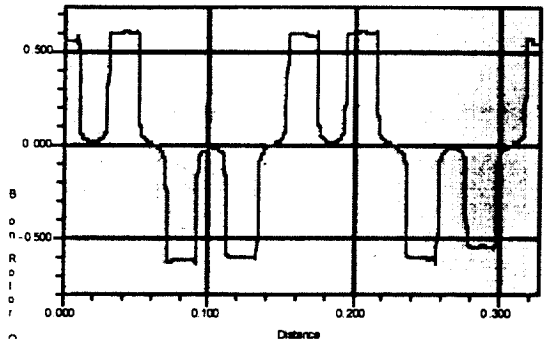

Figure 4 Flux Density on Rotor 8 Pole Pair Bias Configuration

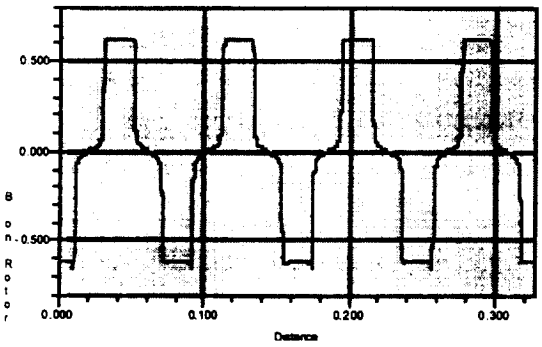

Figure 5 Flux Density on Rotor Alternating 8 Pole Bias Configuration

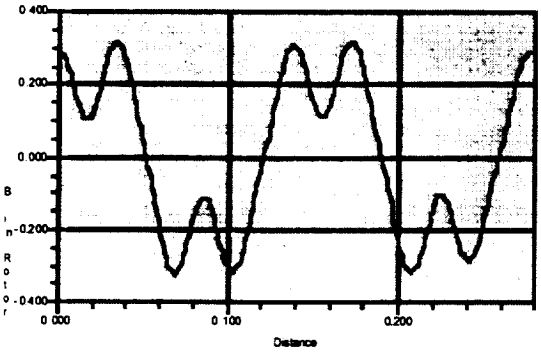

Figure 6 Flux Density in Rotor 8 Pole Pair Bias Configuration

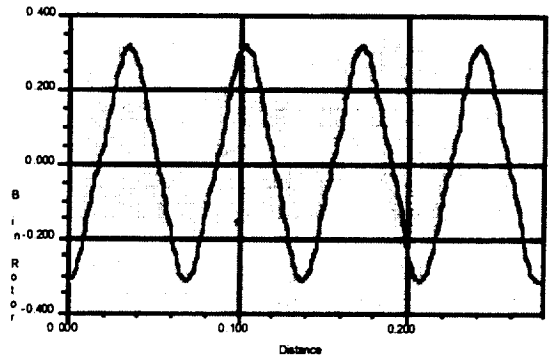

Figure 7 Flux Density in Rotor Alternating 8 Pole Bias Configuration

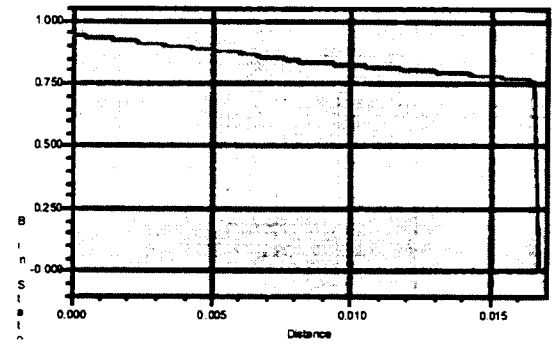

Figure 8 Flux Density in Back Iron 8 Pole Pair Bias Configuration

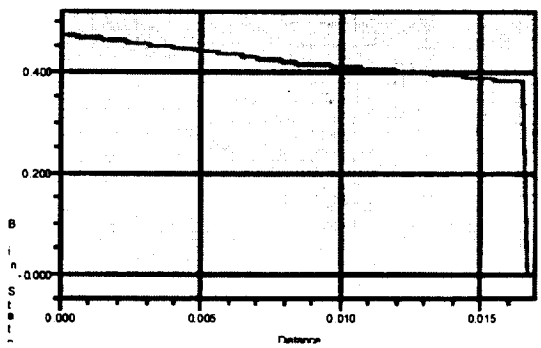

Figure 9 Flux Density in Back Iron Alternating 8 Pole Bias Configuration

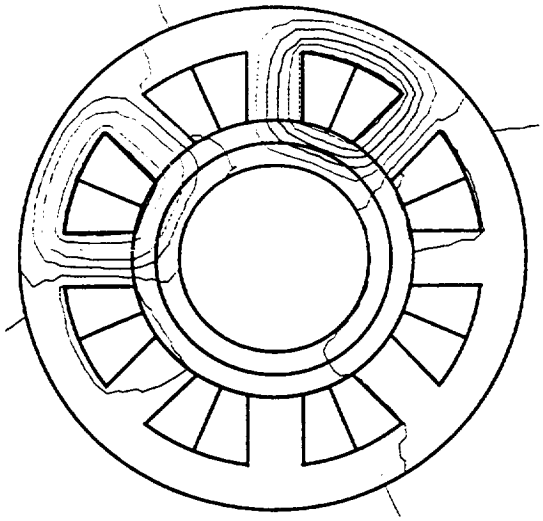

Figure 10 Flux Path for 8 Pole Pair Full Force Configuration

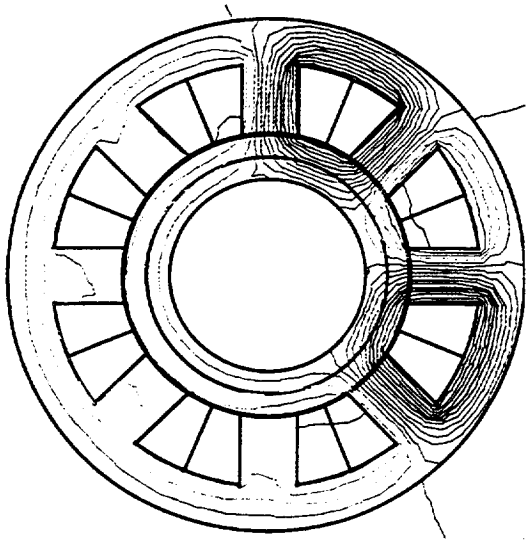

Figure 11 Flux Path for Alternating 8 Pole Full Force Configuration

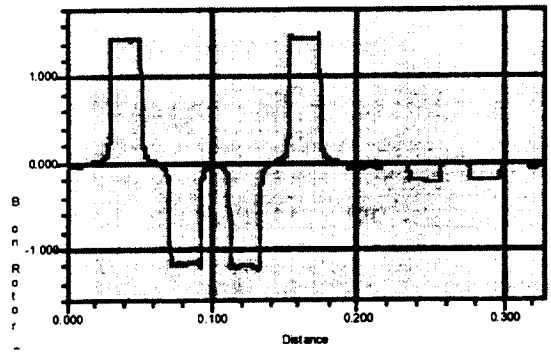

Figure 12 Flux Density on Rotor 8 Pole Pair Full Force Configuration

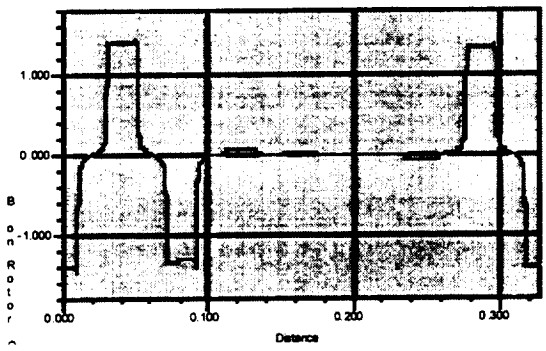

Figure 13 Flux Density on Rotor Alternating 8 Pole Full Force Configuration

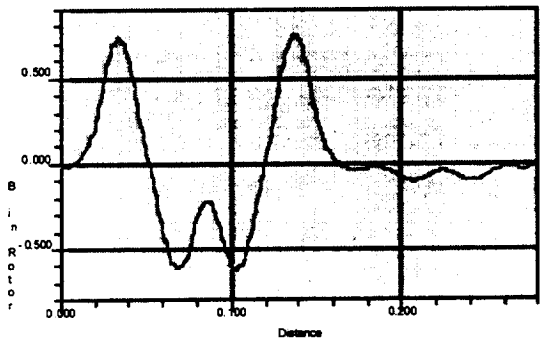

Figure 14 Flux Density in Rotor 8 Pole Pair Full Force Configuration

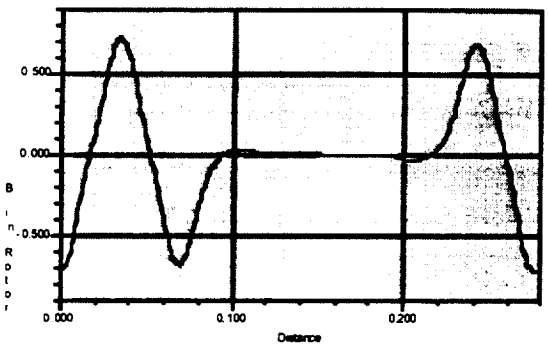

Figure 15 Flux Density in Rotor Alternating 8 Pole Full Force Configuration

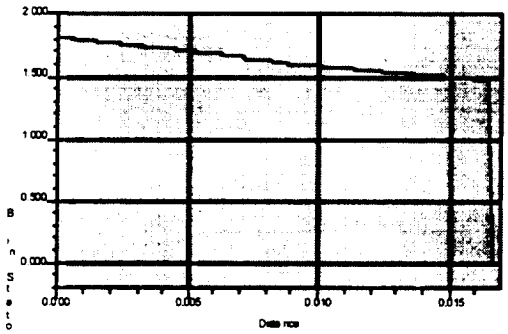

Figure 16 Flux Density in Back Iron 8 Pole Pair Full Force Configuration

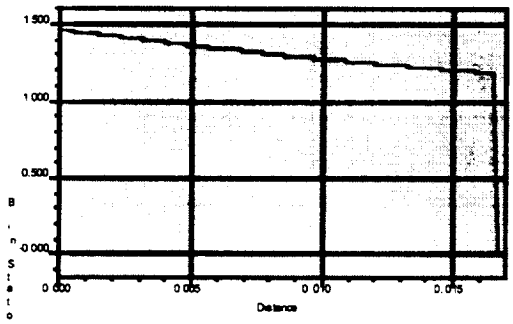

Figure 17 Flux Density in Back Iron Alternating 8 Pole Full Force Configuration

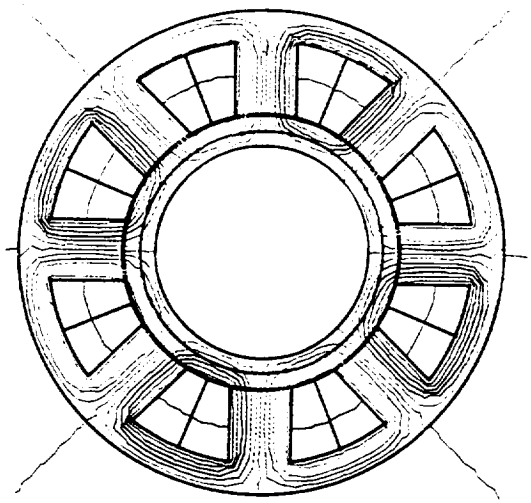

Figure 18 Flux Path for 8 Pole Distributed Bias Flux Configuration

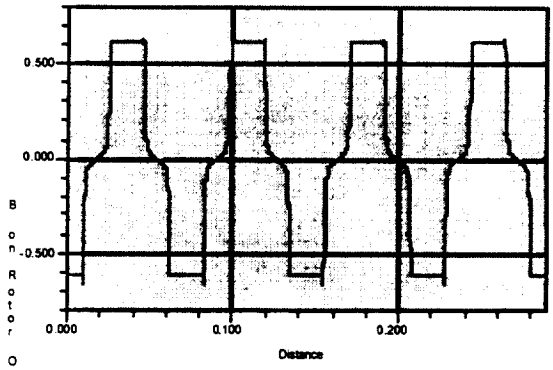

Figure 19 Flux Density on Rotor 8 Pole Distributed Bias Flux Configuration

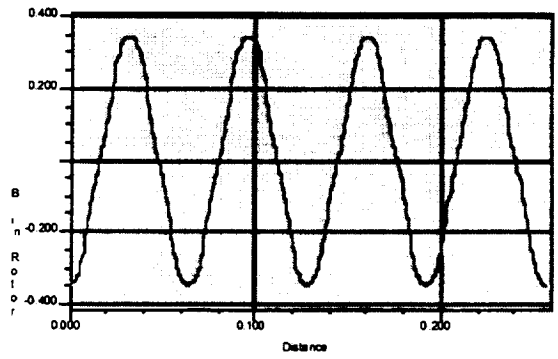

Figure 20 Flux Density in Rotor 8 Pole Distributed Bias Flux Configuration

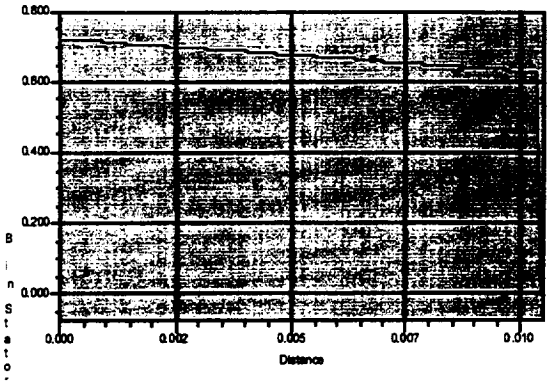

Figure 21 Flux Density in Back Iron 8 Pole Distributed Bias Flux Configuration

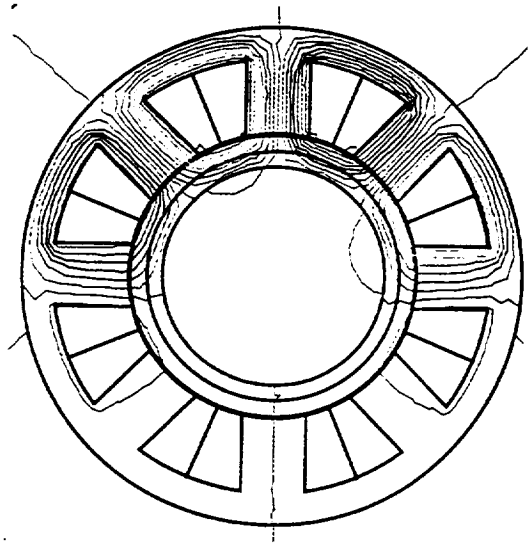

Figure 22 Flux Path for 8 Pole Distributed Flux Full Force Configuration

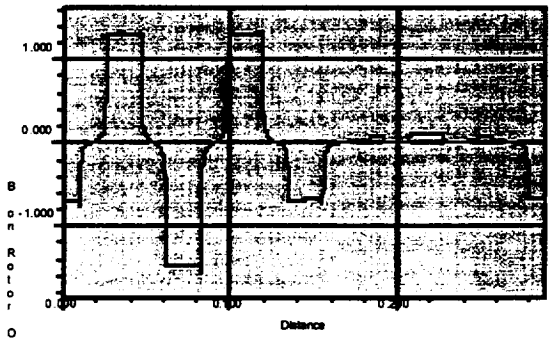

Figure 23 Flux Density on Rotor 8 Pole Distributed Flux Full Force Configuration

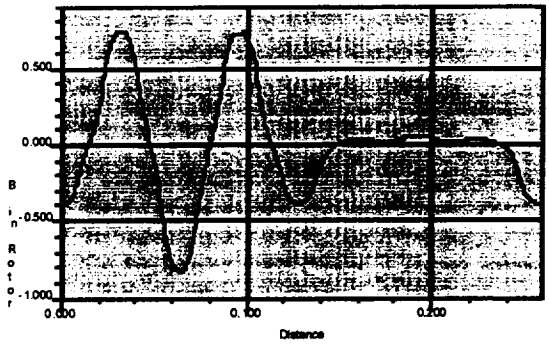

Figure 24 Flux Density in Rotor 8 Pole Distributed Flux Full Force Configuration

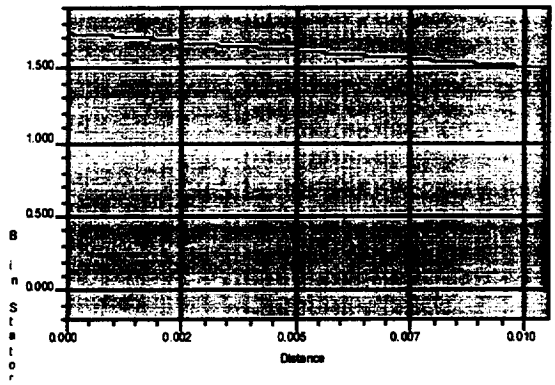

Figure 25 Flux Density in Back Iron 8 Pole Distributed Flux Full Force Configuration

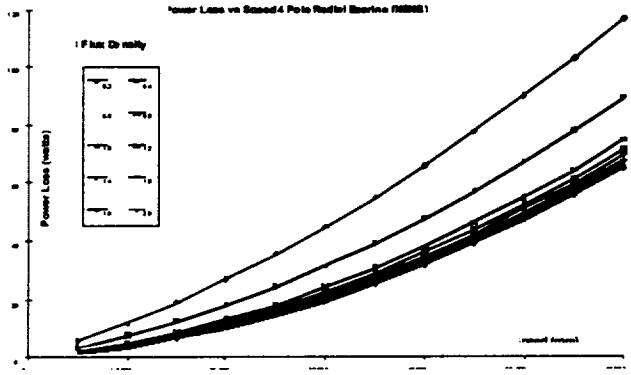

Figure 26 Rotor Loss vs Maximum Control Air Gap Flux Density

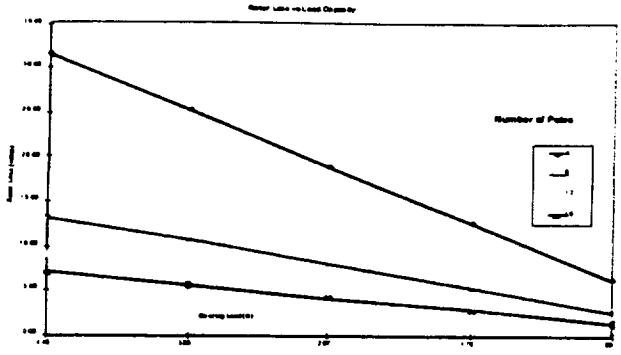

Figure 27 Rotor Loss vs Load Capacity, Speed = 60,000 rpm, Control B = 2.0 Tesla

Table I
8 Pole Magnetic Bearing Dimensions (inches)

	8 Pole Alternating Configuration	8 Pole Pair Configuration	8 Pole Distributed Flux Configuration
R0	1.40	1.40	1.40
R1	2.055	2.055	1.815
R2	2.070	2.070	1.830
R3	3.095	3.095	2.790
R4	3.75	3.75	3.20
Pole Width	.82	.82	.82